International Journal of Mass Spectrometry 283 (2009) 222–228

Contents lists available at ScienceDirect

International Journal of Mass Spectrometry

journal homepage: www.elsevier.com/locate/ijms

2-Nitrophenyl aryl sulfides undergo both intramolecular and electrospray-induced intermolecular oxidation of sulfur: An experimental and theoretical case study

Joseph T. Moolayil[a], M. George[a], Daryl Giblin[b,*], Michael L. Gross[b,*]

[a] Department of Chemistry, Sacred Heart College, Thevara, Cochin 682013, Kerala, India
[b] Department of Chemistry, Washington University, One Brookings Drive, St. Louis, MO 63130, USA

ARTICLE INFO

Article history:
Received 13 December 2008
Received in revised form 1 April 2009
Accepted 1 April 2009
Available online 10 April 2009

Keywords:
Intramolecular oxidation
Nitro substituted aromatic sulfide
Density functional theory
Electrospray ionization
MS/MS

ABSTRACT

Aromatic sulfides bearing a nitro group undergo sulfur oxidation upon electrospray ionization in the positive-ion mode. For example, 2-nitrophenyl phenyl sulfide, its *para* nitro isomer, and its chloro and methyl substituted analogs pick up an oxygen atom to afford $[M+H+O]^+$ and $[M+Na+O]^+$ ions upon ESI. Elemental-composition determination and tandem mass spectrometry confirm the reactions. Another oxidation of the sulfur, by the *ortho* nitro group of the $[M+H]^+$ ions, occurs as intramolecular oxygen-transfer processes, evidenced by characteristic losses of SO, SO_2 and $SO_2H^\bullet$, the latter yielding the carbazole radical cation, and the generation of the aryl-SO^+ product ion. The intramolecular oxidation via oxygen transfer from the nitro group to the sulfur was corroborated by molecular modeling. The results substantiate both inter- and intra-molecular oxidation and provide more evidence that care must be taken when analyzing not only methionine-containing peptides but also small sulfides.

1. Introduction

Electrochemical processes occurring in electrospray ionization (ESI) continue to generate considerable interest among mass spectrometrists and ion chemists [1–3]. The generation of oxidizing agents, like OH radicals and oxygen molecules, occurs in the spray as a consequence of the electrolysis of water molecules [4,5]. Electrochemical processes also perturb solution pH and consequently the abundances of positive ions generated in the gas-phase [3]. The electrochemically induced oxidative processes can be advantageous, for example, in the generation of fullerene radical cations in the gas-phase, allowing investigation of their ion/molecule reactions [6]. Other examples include the formation of $[M-H]^+$ ions from easily oxidizable benzofuran derivatives [7], the generation of higher oxidation states of metal ions in dithiocarbamates [8], and the production of closed-shell ions in the ESI of stable aromatic radicals [9]. The yield of oxidation products impacts ionization efficiency and becomes greater when the conditions of ESI are modified so as to exploit the inherent electrochemistry by using a porous flow-through electrode emitter [10].

The most troublesome oxidation in proteomics occurs where the methionine sulfur in peptides and proteins is converted to a sulfoxide, yielding an $[M+H+O]^+$ at 16 m/z higher than expected [11,12]. Experiments conducted by using ^{18}O labeled water as solvent revealed that the source of oxygen to form the methionine sulfoxide is water [11]. We note that some of the example oxidative processes appear to involve the direct abstraction of an electron [6,8,9], whereas others [7,11] involve a process whereby the oxidation number of functional group is raised [13]. For example, in the case of methionine oxidation, the oxidation number of the functional group containing sulfur is raised by an oxygen transfer.

We report here two different oxidation reactions of the sulfur atoms in the 2-nitrophenyl aryl sulfides (the aryl sulfides **1**–**4** investigated here are given in Scheme 1) observed in these molecules ionized by electrospray. The first class of oxidation of sulfur occurs by oxygen addition, which results from electrochemical oxidation inherent in positive-ion ESI, to form presumably a sulfoxide $[M+H+O]^+$ species. A second, more subtle oxidation of sulfur takes place as an intramolecular process, whereupon activation either in the ionization process itself or by collisional activation (CA), the sulfur is oxidized and the nitro group is reduced via oxygen transfer between these moieties. Evidence for this latter process comes from accurate mass measurements, studies of reference compounds, MS/MS, and molecular modeling. The results complement our continuing studies of nitro aromatic compounds [14]. Uniting the two are processes that raise the oxidation state of the sulfur atom.

Indeed, aromatic sulfides are susceptible to oxidation under mild conditions on the timescale of minutes under microwave irra-

* Corresponding authors.
E-mail address: mgross@wustl.edu (M.L. Gross).

1387-3806/$ – see front matter © 2009 Elsevier B.V. All rights reserved.
doi:10.1016/j.ijms.2009.04.003

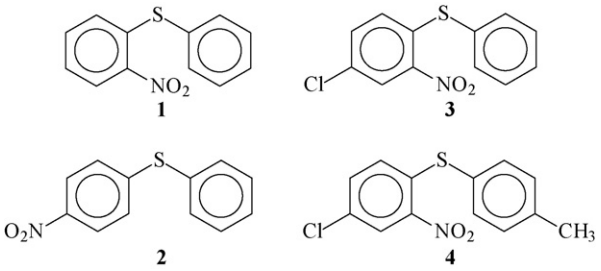

Scheme 1. Structures of the sulfides.

diation [15]. Intramolecular oxidation of sulfur via oxygen transfer from a proximal nitro group [16] occurs for radical cations, leading to surprising fragmentations (e.g., loss of SO_2 from protonated 2-nitrophenyl-4-tolyl sulfide in EI-MS [17] and the formation of $C_6H_5SO_2^+$ from protonated 2-phenylthio-3-nitropyridine [18]). In addition, oxidation of selenium analogs via hydroxyl transfer from a protonated proximal nitro moiety was reported [17]. A mechanism of elimination of SO_2 involving both oxygen and phenyl migration without further cyclization was proposed and buttressed with rudimentary calculations using DFT theory [19]. The purpose of this research is to see if both an intermolecular oxidation and an analogous intramolecular oxidation occur for ESI-generated, closed-shell $[M+H]^+$ ions and to explore the mechanisms for the reactions.

2. Experimental

2.1. Synthesis

Sulfides **1**–**4** (Scheme 1) were synthesized from the appropriate chloronitrobenzenes and thiophenol by using reported procedures [19]. Purity of the samples was checked by TLC, and the structures were confirmed by NMR, IR, and mass-spectrometric analyses, as described earlier [14]. Carbazole used for this study was purchased from Aldrich Chemical Co. (Milwaukee, WI) and used without further purification.

2.2. Mass spectrometry

ESI experiments were conducted by using a Micromass Q-Tof-*Ultima* (Waters, Manchester, UK) instrument operated in the positive-ion mode. The metallic needle voltage was 3 kV, and the cone voltage was 90 V. The temperatures of the source block and for desolvation were 90 and 150 °C, respectively. The samples were dissolved in 1:1 mixture of acetonitrile and water containing 1% formic acid. The samples were introduced by direct infusion at a flow rate of 10 μL/min. All parameters (i.e., aperture to the TOF, transport voltage, offset voltages) were optimized to achieve maximum sensitivity and a mass resolving power of 15,000 in the "*w*" mode (full width at half maximum). The CAD experiments were carried out by mass selecting the precursor ion by using the quadruple analyzer and collisionally activating the selected ion in a quadrupole collision chamber that follows; the product ions were recorded by using the time-of-flight analyzer. Collision voltages for fragmenting the precursor ions were in the range of 7–10 V. Accurate masses of the product ions were determined by using the precursor ion as the internal mass standard.

Some ESI-MS and low-energy MS/MS and MS3 experiments were performed by using a Thermo Finnigan LCQ Advantage or a Thermo Finnigan LCQ Classic 3D ion-trap mass spectrometers (San Jose, CA).

For high-energy experiments, ions were generated by CI (chemical ionization) using methane as the reagent gas. The CI–MI (metastable ion) and high-energy CA experiments were conducted on a VG ZAB-T four-sector mass spectrometer of BEBE design [20]. Samples were introduced through a heated direct-insertion probe with source temperature of 200 °C. MS1 was a standard high-resolving power, and double-focusing mass spectrometer (ZAB) of reverse geometry. MS2 possessed a prototype Mattauch–Herzog-type design, incorporating a standard magnet and a planar electrostatic analyzer having an inhomogeneous electric field, followed by single-point and array detectors. Ions were accelerated to 8 kV and subjected to collisions at 4 keV in the third field-free region and detected at the single-point detector. Data acquisition and workup were accomplished by using a VAX 3100 work-station equipped with OPUS software (VG, Manchester, England).

2.3. Theoretical calculations

Initial scans for candidates and connections on potential energy surfaces for protonated 2-nitropheyl-phenyl sulfide and sulfoxide were performed by using the PM3 [21,22] semi-empirical algorithm (Spartan '02 for Linux, Wave function Inc.) for computational efficiency. Additional scans of the potential surface were performed by using density functional theory (B3LYP). Geometric optimization of candidate minima and transition states were performed by using density functional theory (DFT; B3LYP/6-31G (d, p) level), which required less computational overhead than do formal *ab initio* methods and yet incorporated dynamic correlation, has little spin contamination [23–25], and usually performed adequately giving proper geometries, energies, and frequencies [26]. DFT was part of the Gaussian 03/98 suites (Gaussian Inc.) [27,28]. The optimized minima and transition states were confirmed by vibration frequency analysis. Connections of transition states to minima were analyzed by combination of inspection, projection along normal reaction coordinates, or reaction-path calculations as needed; also discovered by the reaction-path calculations were ion–dipole complexes. Final single-point energies were calculated at the B3LYP/6-311+G (2d, p)//B3LYP/6-31G (d, p) level, scaled thermal-energy corrections for standard conditions derived from the frequency calculations were applied [29], and reported as relative enthalpies in kcal/mol.

3. Results and discussion

3.1. ESI-induced intermolecular oxidation

The ESI mass spectrum of 2-nitrophenyl phenyl sulfide **1** shows an $[M+H]^+$ ion of *m*/*z* 232 and another ion of *m*/*z* 248, 16 *m*/*z* higher (Fig. 1). The measured accurate mass for the ion of *m*/*z* 248 is 248.0381, which agrees within 2 ppm of the accurate mass calculated for the $[M+H+O]^+$ ion, $C_{12}H_{10}NO_3S$ (Table 1). That ion of *m*/*z* 248, $[M+H+O]^+$, is likely the $[M+H]^+$ ion of the sulfoxide generated by an oxygen-transfer process initiated by generation of intermediate oxidizing species at the emitter electrode of the ESI source [4,5]. The ions of *m*/*z* 254, 270, and 286 are the analogous $[M+Na]^+$, $[M+Na+O]^+$ likely contaminated with minor isobaric $[M+K]^+$, and $[M+K+O]^+$ ions, respectively, of **1** (Table 1) where Na^+ or K^+ has replaced the proton as the ionizing agent.

To confirm the structure assigned for the ion of *m*/*z* 248, its CAD mass spectrum (Fig. 2a) was compared with that of the authentic sulfoxide of sulfide **1** (Fig. 2b). That standard was produced by a standard oxidation procedure of sulfide **1** by using sodium periodate and introduced to the spectrometer by ESI [30]. The two spectra are virtually identical, confirming the proposed structure produced by ESI-induced electrochemical oxidation of sulfide **1** in the ion source. The elemental compositions of the fragment ions were assigned based on high-mass resolving power (~15,000), and

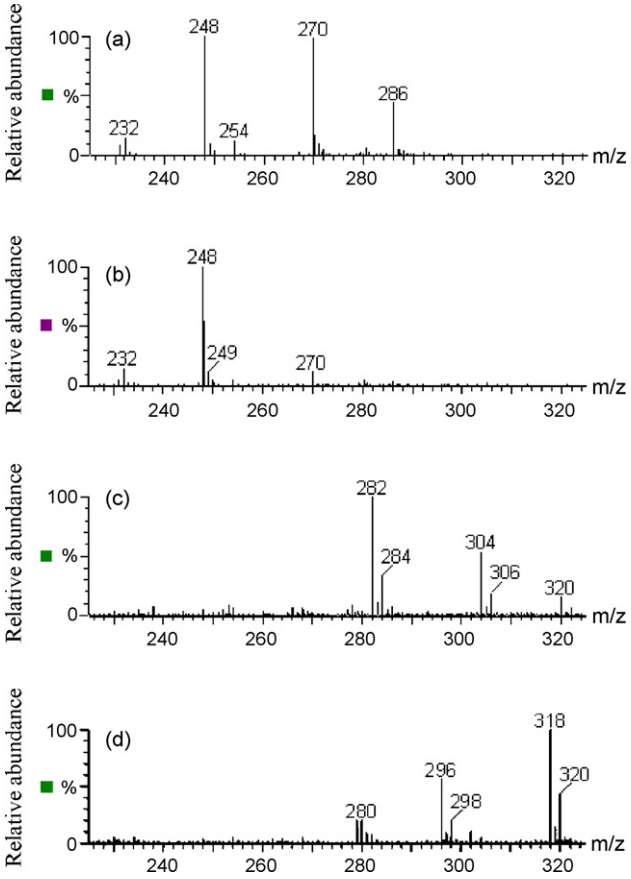

Fig. 1. ESI mass spectra of (a) sulfide **1** (b) sulfide **2** (c) sulfide **3** (d) sulfide **4**. The figures show $[M+H]^+$, $[M+H+O]^+$ and $[M+Na+O]^+$ ions.

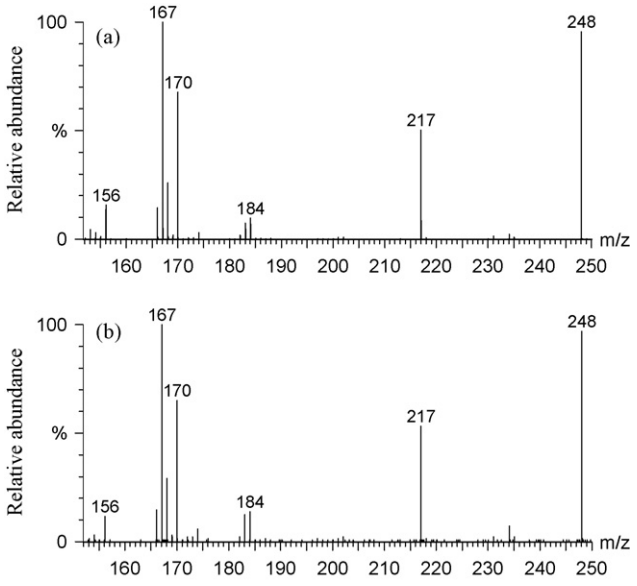

Fig. 2. The CAD mass spectra of ions of *m/z* 248 (a) oxidation product of sulfide **1** and (b) $[M+H]^+$ of sulfoxide.

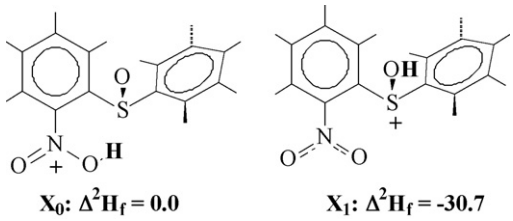

Scheme 2. Preferred structure of *m/z* 248.

accurate mass data (Table 1) obtained in the MS/MS mode, taking the precursor ion as the mass standard.

Calculations by DFT reveal that the preferred site of protonation to form the $[M+H]^+$ of the mono-oxidized species is at the oxygen on the sulfur (Scheme 2), in contrast to one of the nitro-group oxygens as is the case for the $[M+H]^+$ of the unoxidized species [14]. Indeed, the SO site is preferred over the oxygens of the nitro group by >30 kcal/mol. Major fragment ions, observed in the CAD spectra, are of *m/z* 217, $[M+H-HNO]^+$; 184, $[M+H-SO_2]^+$; 170 $[M+H-C_6H_6]^+$; and 167 $[M+H-(SO_2+OH)]^{+\bullet}$. Note that the losses of SO_2 and (SO_2+OH•) would require a transfer of an oxygen from the nitro group to the sulfur atom. The overall envelop of fragments is distinct from that observed for the protonated sulfides (Fig. 3), indicating that the sulfoxide, because of a different site for initial protonation, has available to it different routes of fragmentation.

The ESI mass spectra of sulfides **2**–**4** (Fig. 1b–d, Table 1) show features similar to that for 2-nitrophenyl phenyl sulfide **1** including the ESI-induced oxidation in all cases. The measured accurate masses of the proposed $[M+H+O]^+$ ions (Table 1) agree closely with the expected elemental compositions; also produced by ESI were the adducts, $[M+Na]^+$, $[M+Na+O]^+$, and $[M+K+O]^+$ ions (Table 1). The CAD mass spectra of the ESI-generated $[M+H+O]^+$ ions (Table 2) show that sulfides **1**, **3**, and **4** fragment similarly; whereas, sulfide **2**, which has a *para* nitro group instead, does not undergo the prominent losses of HNO, SO_2 and (SO_2+OH•) but instead loses OH• (to give an ion of *m/z* 231) and NO_2•(to give an ion of *m/z* 202). Thus, the

Table 1
Measured accurate masses of the ESI oxidation products from sulfides **1**–**4**.

Compound	Ion	Molecular formula for ion	Measured mass	Calculated mass	Deviation (ppm)
1	$[M+H+O]^+$	$C_{12}H_{10}NO_3S$	248.0377	248.0381	−2
2	$[M+H+O]^+$	$C_{12}H_{10}NO_3S$	248.0387	248.0381	2
3	$[M+H+O]^+$	$C_{12}H_9NO_3SCl$	281.9991	281.9992	−0.4
4	$[M+H+O]^+$	$C_{13}H_{11}NO_3SCl$	296.0143	296.0148	−2
1	$[M+Na]^+$	$C_{12}H_9NOSNa$	254.0253	254.0246	2.6
1	$[M+Na+O]^+$	$C_{12}H_9NO_3SNa$	270.0175	270.0195	−7.5
	$[M+K]^+$	$C_{12}H_9NO_2SK$		269.9986	70
2	$[M+Na+O]^+$	$C_{12}H_9NO_3SNa$	270.0182	270.0195	−4.9
3	$[M+Na+O]^+$	$C_{12}H_8NO_3SClNa$	303.9811	303.9808	0.8
4	$[M+Na+O]^+$	$C_{13}H_{10}NO_3SClNa$	317.9898	317.9962	−20
	$[M+K]^+$	$C_{13}H_{10}NOSClK$		317.9752	46
1	$[M+K+O]^+$	$C_{12}H_9NO_3SK$	285.9940	285.9948	−2.7
2	$[M+K+O]^+$	$C_{12}H_9NO_3SK$	285.9940	285.9947	−2
3	$[M+K+O]^+$	$C_{12}H_8NO_3SClK$	319.9583	319.9545	12
4	$[M+K+O]^+$	$C_{13}H_{10}NO_3SClK$	333.9703	333.9701	0.4

Table 2
Partial CAD mass spectra of $[M+H+O]^+$ ions derived by ESI of sulfides **1**–**4**.

Precursor	Measured accurate masses of fragment ions due to loss of X, elemental composition and abundances in parenthesis.				
	$X = HNO$	$X = SO_2$	$X = C_6H_6$	$X = SO_2 + OH^•$	Other ions
Sulfoxide **1** *m/z* 248	217.0325 $C_{12}H_9O_2S$ (52)	184.0767 $C_{12}H_{10}NO$ (12)	169.9906 $C_6H_4NO_3S$ (68)	167.0725 $C_{12}H_9N$ (100)	*m/z* 183 (18) 168 (25)
Sulfoxide **2** *m/z* 248	ND	ND	169.9906 $C_6H_4NO_3S$ (35)	ND	*m/z* 202(100) 231(75)
Sulfoxide **3** *m/z* 282	250.9930 $C_{12}H_8O_2SCl$ (50)	218.0357 $C_{12}H_9NOCl$ (10)	203.9512 $C_6H_3NO_3SCl$ (90)	201.0340 $C_{12}H_8NCl$ (100)	*m/z* 183(42) 167(65)
Sulfoxide **4** *m/z* 296	265.0098 $C_{13}H_{10}O_2SCl$ (12)	232.0494 $C_{13}H_{11}NOCl$ (70)	203.9520 $C_6H_3NO_3SCl$ (100)	215.0499 $C_{13}H_{10}NCl$ (65)	*m/z* 214(75) 180(90)

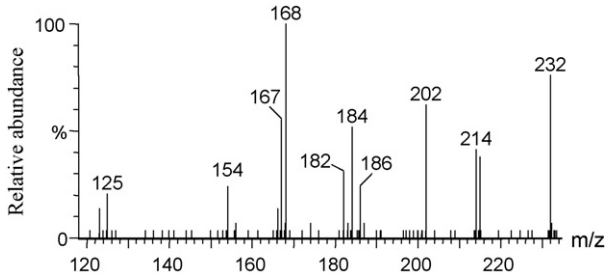

Fig. 3. CAD mass spectrum of ESI produced $[M+H]^+$ ion of sulfide **1**.

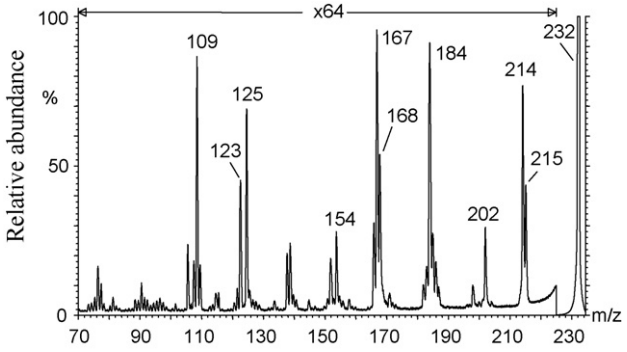

Fig. 4. MI mass spectrum of CH_4 CI produced $[M+H]^+$ ion of sulfide **1** (BEBE instrument).

losses of HNO, SO_2 and (SO_2+$OH^•$) require the proximal *ortho* nitro group, and the losses of SO_2 and (SO_2+$OH^•$) additionally require the transfer of an oxygen, which we view as an intramolecular oxidation. In addition, the $[M+H+O]^+$ ions generated from sulfides **1**–**3** dissociate by the elimination of a molecule of C_6H_6 whereas that of sulfide **4**, having a methyl group at the 4′-position, expels a molecule of $C_6H_5CH_3$, consistent with the assignment that they are indeed sulfoxides.

3.2. Intramolecular oxidation

ESI-protonated 2-nitrophenyl phenyl sulfide **1** produces, upon collisional activation, fragment ions of *m/z* 215, 214, 202, 186, 184 168, 167, 154, 125, 123 (Fig. 3) and *m/z* 109 (not shown). The ions of *m/z* 215 and 214 arise by the losses of an OH radical and H_2O, respectively; we described the mechanisms of these fragmentations earlier [13]. The unusual ions of *m/z* 202, 168 and 167 are formed by eliminations of $NO^•$, SO_2 and $SO_2H^•$, respectively, from the $[M+H]^+$. The product ions of *m/z* 154, 125, 123, and 109 are $C_6H_4NO_2S^+$, $C_6H_5SO^+$, $C_6H_5NO_2^+$, and likely $C_6H_5S^+$, respectively. The isobaric fragment ions of *m/z* 184 arise by the expulsion of either SO or the elements of H_2NO_2 from the $[M+H]^+$ ion; selection of *m/z* 234 as the $[M+H]^+$ ion, using the native ^{34}S isotope, reveals that both are major losses. The *m/z* 186 ion arises from the sequential loss of H_2O and CO from the $[M+H]^+$ ion, as previously reported [13]. Furthermore, MS^3 studies of the product ions of *m/z* 184 and 168 reveal further dissociations by losses of OH and H radicals, respectively, to generate *m/z* 167. Moreover, the CAD mass spectrum of the *m/z* 167 fragment is virtually identical to that of the radical cation of carbazole, indicating that *m/z* 167 product ion is indeed the carbazole radical cation and is formed in violation of the even-electron ion rule. Accurate mass measurements of the fragment ions, obtained under high-mass resolving power as described in Section 2, verify the formulae of the product ions and losses in the eliminations (Table 3).

For comparison, we produced protonated 2-nitrophenyl phenyl sulfide **1** by CH_4 CI (Section 2); this ionization does not produce the $[M+O+H]^+$ ion. The MI spectrum of the CI-generated $[M+H]^+$ ion is shown in Fig. 4; the CAD spectrum of the same precursor is similar but shows enhanced abundances of lower *m/z* fragment ions (not shown). Whichever the ionization mode is, CAD produces the same series of fragment ions but in somewhat different abundances. In addition, it appears that the CH_4 CI ions are produced with more internal energy than the ESI-produced ions.

The abundances of ions from the losses of $NO^•$, SO, SO_2, and $SO_2H^•$ are summarized in Table 3 for the CAD spectra for the ESI-produced $[M+H]^+$ ions of sulfides **1**–**4**. We note that losses of SO, SO_2, and $SO_2H^•$ are absent in the CAD spectra for the ESI-produced $[M+H]^+$ ion of sulfide **2**, which has a *para* rather than an *ortho* nitro group. Consistent also with oxidation of S are the aryl-SO^+ ions formed upon CAD of the $[M+H]^+$ ions of sulfides **1**, **3**, and **4**. On this basis, we surmise that the expulsions of SO, SO_2, and the SO_2H radical from the $[M+H]^+$ ions arise after transfer of one or two oxygen atoms from the nitro group to the sulfur atom rather than by an abstraction in the final elimination step. In addition, given that the *m/z* 167 ion is the tricyclic carbazole radical cation, it is likely that cyclization takes place as a consequence of this intramolecular oxidation of sulfur, and is driven by the internal energy of the ions. The two *m/z* 184 ions, which arise by losses of both SO and the elements of NO_2H_2 (likely H_2O + NO), were unresolved with respect to model ions because of lack of necessary precursor ion resolving power. To elucidate further the mechanism of the necessary rearrangements and subsequent eliminations of SO, SO_2 and SO_2H radical, we

Table 3
Partial CAD mass spectra of $[M+H]^+$ ions produced by ESI from sulfides **1**–**4**.

Precursor	Measured accurate masses of fragment ions due to loss of X, elemental composition and abundances in parenthesis.				
	$X = NO^•$	$X = SO$	$X = SO_2$	$X = SO_2H^•$	Other ions
Sulfide **1** *m/z* 232	202.0463 $C_{12}H_{10}OS$ (66)	184.0769 $C_{12}H_{10}NO$ (66)	168.0815 $C_{12}H_{10}N$ (100)	167.0732 $C_{12}H_9N$ (40)	184.0343 $C_{12}H_8S$ (<1%) $[M+H-NO_2H_2]^+$
Sulfide **2** *m/z* 232	202.0463 $C_{12}H_{10}OS$ (65)	ND	ND	ND	184.0349 $C_{12}H_8S$ (3) $[M+H-NO_2H_2]^+$
Sulfide **3** *m/z* 266	236 $C_{12}H_9OSCl$ (10)	218 $C_{12}H_9NOCl$ (13)	202 $C_6H_3NO_2Cl$ (9)	201 $C_{12}H_8NCl$ (15)	*m/z* 167(100) $[M+H-SO_2-Cl]^+$
Sulfide **4** *m/z* 280	250 $C_{13}H_{10}O_2SCl$ (5)	232.0494 $C_{13}H_{11}NOCl$ (18)	214. $C_6H_3NO_3SCl$ (13)	215 $C_{13}H_{10}NCl$ (25)	*m/z*181(100) $[M+H-SO_2-Cl]^+$

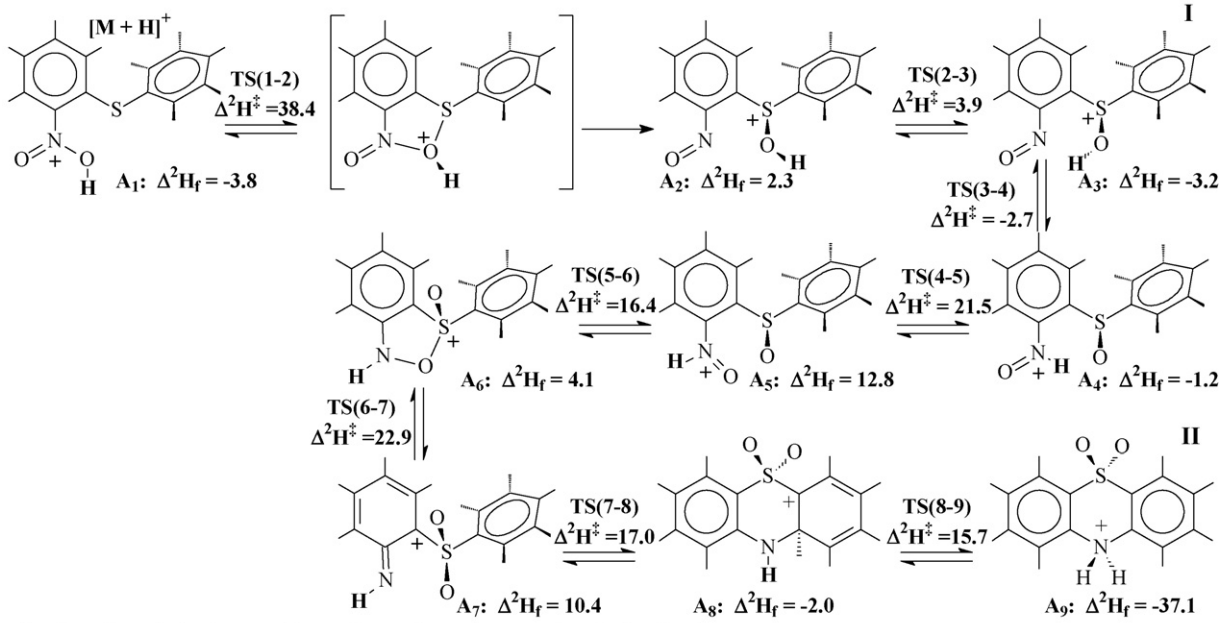

All values for relative heats of formation and reaction are given in kcal/mol.
Zero point for relative heats of formation is the $\mathbf{A_0}$ conformer for consistency with and from a previous publication [13].

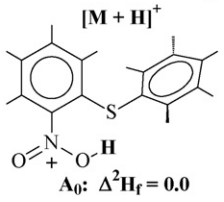

Scheme 3. Proposed mechanism for intramolecular oxidation and cyclization.

carried out molecular orbital calculations by using DFT, as described in Section 2.

3.3. Theoretical calculations

We discovered in scanning the potential energy surface at both low level and DFT that there exists a web of potential routes for the intramolecular oxidation of the sulfur by the nitro group and the formation of characteristic product ions. We selected for presentation the 'best' of the potential routes based on lowest required energy to surmount the greatest transition-state barriers. We report the calculated enthalpies of formation for the intermediates, products and transition states, relative to that of the previously reported $[M+H]^+$ ion [14] in kcal/mol.

Proposed mechanism for intramolecular oxidation of sulfur by two sequential oxygen transfers is shown in Scheme 3. The first step involves the transfer of an OH group from the nitro group to the sulfur atom, affording intermediate **I** ($\mathbf{A_3}$). This first step is presumably rate limiting in that it presents the greatest energetic barrier, **TS** (**1**–**2**), in the scheme. The second round of oxygen transfer involves a stable intermediate, $\mathbf{A_6}$, which decomposes followed by cyclization ultimately leading to the tricyclic intermediate **II** ($\mathbf{A_9}$),

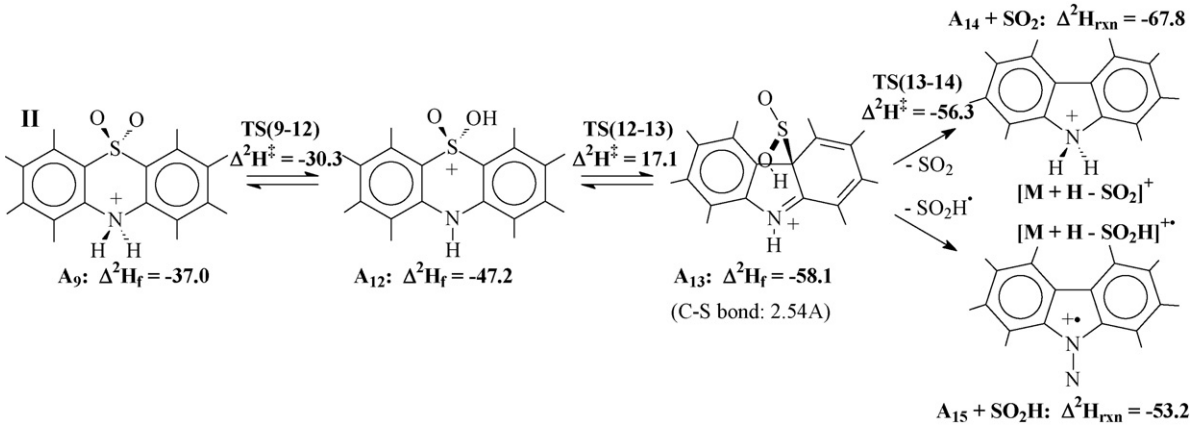

Scheme 4. Proposed mechanism for elimination of SO_2 and SO_2H.

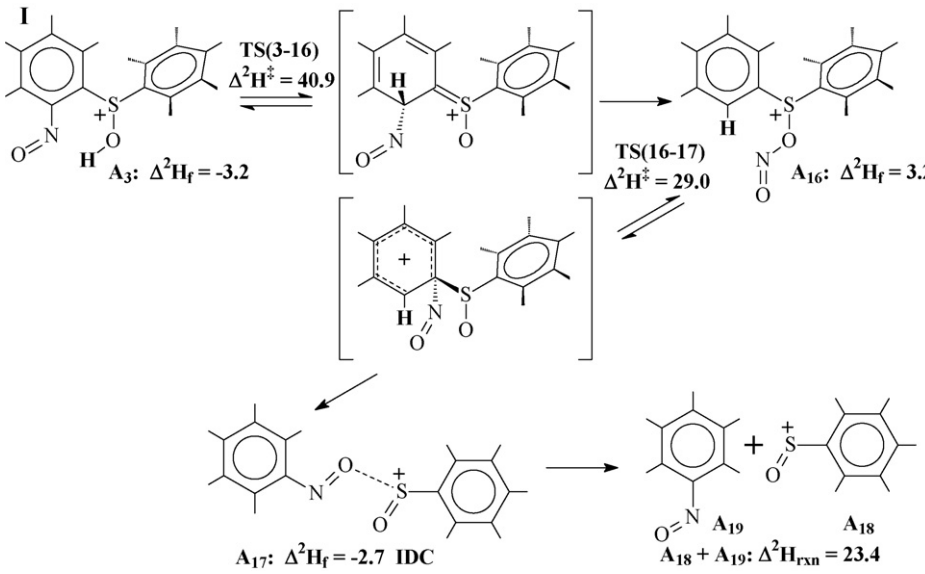

Scheme 5. Proposed mechanism for formation of $C_6H_5SO^+$ (*m/z* 125 ion).

an energetically favorable form ($\Delta^2H_f = -37.1$ kcal/mol) in which both oxygens are now attached to the sulfur, and the nitro group has been consequently reduced to a secondary amine.

The route to the expulsions of SO_2 and the SO_2H radical starts from intermediate **II** (Scheme 4) and proceeds through the metastasis of a carbon–sulfur bond to a carbon–carbon bond yielding a tricyclic intermediate with a five-membered ring, $\mathbf{A_{13}}$. We propose that this intermediate, which features a long C–S bond of 2.54 Å, can decompose to yield the heterocyclic fragments of *m/z* 168 and 167 (protonated carbazole and a carbazole radical cation, respectively, the latter being experimentally verified). In addition, the intermediate **I**, formed by the transfer of one oxygen atom from the nitro group to sulfur, is also the starting point for the formation of the *m/z* 125 ion ($C_6H_5SO^+$), as shown in Scheme 5. A critical and significant feature of this route to the product ion involves sequential NO• migrations that are more energetically favorable than any H or OH migration we discovered. Additionally, the exit channel features a prominent ion–neutral complex between the phenyl-SO^+ product ion and nitrosobenzene.

The proposed route for SO loss is analogous to that for SO_2 loss and involves an intramolecular transfer of oxygen from the protonated nitro group to the sulfur via a cyclic intermediate, $\mathbf{A_{20}}$, which is just a shoulder on the transfer pathway (Scheme 6). This is followed by cyclization and proton transfer to form an energetically favorable tricyclic intermediate, $\mathbf{A_{23}}$ ($\Delta^2H_f = -29.0$ kcal/mol). The expulsion of SO commences from intermediate $\mathbf{A_{23}}$ via the metas-

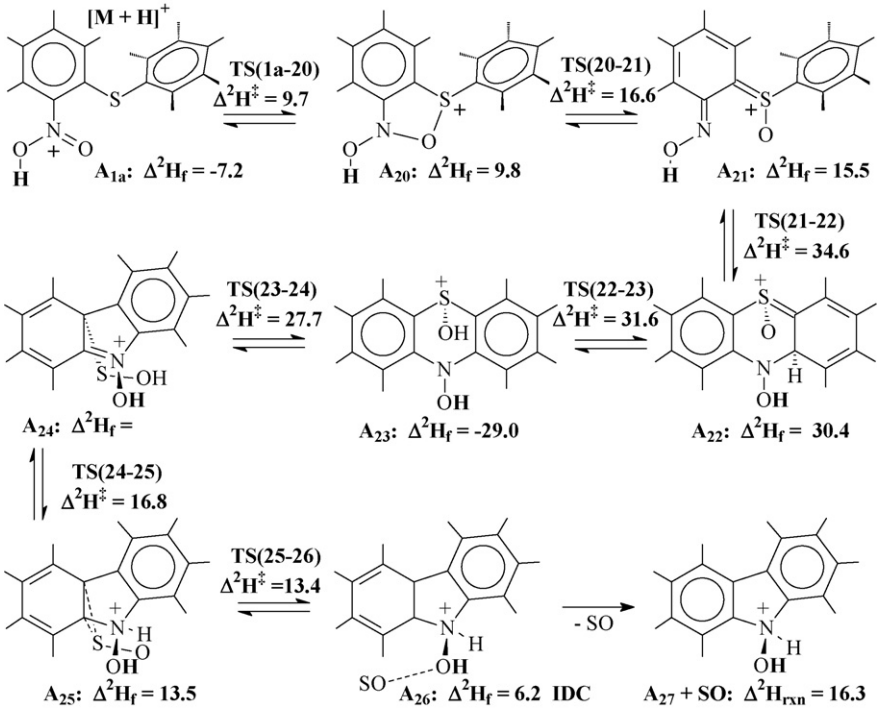

Scheme 6. Proposed mechanism for elimination of SO.

tasis of a carbon–sulfur bond to a carbon–carbon bond, yielding a tricyclic intermediate with a five-membered ring, $\mathbf{A_{24}}$, which decomposes by SO loss (Scheme 6) through an ion–dipole complex. We note that in all the proposed schemes, the maximum barrier at a transition state is ~40 kcal/mol, which is also consistent with previously proposed mechanisms for other fragmentations of the these sulfides (**1**–**4**).

4. Conclusion

ESI of 2-nitrophenyl phenyl sulfide, the chloro and methyl substituted analogs, and its *para* nitro isomer all undergo oxygen atom addition in an ESI source during ionization. The products formed are sulfoxides, as characterized by tandem mass-spectrometric experiments and accurate mass measurements. Additionally, those ESI-protonated aromatic sulfides containing *ortho* nitro groups also show oxidation of sulfur by internal oxygen transfer. Evidence includes the characteristic expulsions of SO, SO_2 and the SO_2H radical, and the production of aryl-SO^+. We view this chemistry as a second class of oxidation, an intramolecular oxidation of the sulfur atom with reduction of the nitro group via transfer of oxygen atoms. The mechanisms for transfer and consequent fragmentation were substantiated by molecular modeling using DFT theory.

Acknowledgements

J.T.M and M.G. thank the KSCSTE for financial assistance and Principal, S.H. College, Thevara for providing infrastructure. Research at WU was supported by the National Centers for Research Resources of the NIH, Grant P41RR000954. This work made use of the Washington University Computational Chemistry Facility, supported by NSF grant CHE-0443501.

Appendix A. Supplementary data

Supplementary data associated with this article can be found, in the online version, at doi:10.1016/j.ijms.2009.04.003.

References

[1] L. Li, C. Huang, Electrochemical/electrospray mass-spectrometric studies of electrochemically stimulated ATP release from PP/ATP films, J. Am. Soc. Mass Spectrom. 18 (5) (2007) 919–926.
[2] J.F. De La Mora, G.J. Van Berkel, C.G. Enke, R.B. Cole, M. Martinez-Sanchez, J.B. Fenn, Electrochemical processes in electrospray ionization mass spectrometry, J. Mass Spectrom. 35 (8) (2000) 939–952.
[3] G.J. Van Berkel, F. Zhou, J.T. Aronson, Changes in bulk solution pH caused by the inherent controlled-current electrolytic process of an electrospray ion source, Int. J. Mass Spectrom. Ion Processes 162 (1–3) (1997) 55–67.
[4] S. Liu, W.J. Griffiths, J. Sjoevall, On-column electrochemical reactions accompanying the electrospray process, Anal. Chem. 75 (4) (2003) 1022–1030.
[5] R.A. Ochran, L. Konermann, Effects of ground loop currents on signal intensities in electrospray mass spectrometry, J. Am. Soc. Mass Spectrom. 15 (12) (2004) 1748–1754.
[6] D. Rondeau, D. Kreher, M. Cariou, P. Hudhomme, A. Gorgues, P. Richomme, Electrolytic electrospray ionization mass spectrometry of C(60)-TTF-C(60) derivatives: high-resolution mass measurement and molecular ion gas-phase reactivity, Rapid Commun. Mass Spectrom. 15 (18) (2001) 1708–1712.
[7] T. Karancsi, P. Slegel, L. Novak, G. Pirok, P. Kovacs, K. Vekey, Unusual behavior of some isochromene and benzofuran derivatives during electrospray ionization, Rapid Commun. Mass Spectrom. 11 (1) (1997) 81–84.
[8] D.F. Schoener, M.A. Olsen, P.G. Cummings, C. Basic, Electrospray ionization of neutral metal dithiocarbamate complexes using in-source oxidation, J. Mass Spectrom. 34 (10) (1999) 1069–1078.
[9] J.O. Metzger, J. Griep-Raming, Electrospray ionization and atmospheric pressure ionization mass spectrometry of stable organic radicals, Eur. Mass Spectrom. 5 (3) (1999) 157–163.
[10] Gary J. Van Berkel, Vilmos Kertesz, Michael J. Ford, Michael C. Granger, Efficient analyte oxidation in an electrospray ion source using a porous flow-through electrode emitter, J. Am. Soc. Mass Spectrom. 15 (12) (2004) 1755–1766.
[11] M. Chen, K.D. Cook, Oxidation artifacts in the electrospray mass spectrometry of Aβ peptide, Anal. Chem. 79 (5) (2007) 2031–2036.
[12] K.P. Bateman, Electrochemical properties of capillary electrophoresis-nanoelectrospray mass spectrometry, J. Am. Soc. Mass Spectrom. 10 (4) (1999) 309–317.
[13] J. March, "Oxidation and reductions", in: Advanced Organic Chemistry, fourth ed., Wiley Interscience, New York, 1992, p. 1158.
[14] J.T. Moolayil, M. George, R. Srinivas, A.L. Russell, D. Giblin, M.L. Gross, Protonated nitro group as a gas-phase electrophile: experimental and theoretical study of the cyclization of *o*-nitrodiphenyl ethers, amines, and sulfides, J. Am. Soc. Mass Spectrom. 18 (12) (2007) 2204–2217.
[15] I. Mohammadpoor-Baltork, H.R. Memarian, K. Bahrami, 3-Carboxypyridinium chlorochromate-aluminum chloride—an efficient and inexpensive reagent system for the selective oxidation of sulfides to sulfoxides and sulfones in solution and under microwave irradiation, Can. J. Chem. 83 (2) (2005) 115–121.
[16] D.V. Ramana, N. Sundaram, M. George, Ortho effects in organic molecules on electron impact. Part 22. Competing oxygen transfers from the nitro group to sulfur and the olefinic double bond in 2-nitrophenyl styryl sulfides, Org. Mass Spectrom. 25 (3) (1990) 161–164.
[17] J. Martens, K. Praefcke, U. Schulze, H. Schwarz, H. Simon, Spectroscopic investigations. XI. Organic selenium compounds. I. electron impact induced oxygen or hydroxyl group transfer to selenium functions, Tetrahedron 32 (20) (1976) 2467–2472.
[18] F. El-Zahara, M. El-Hegazy, M.E. Mahmoud, E.F. Saad, E.A. Hamed, Mass spectral study of some phenyl mono- and dinitro-pyridyl sulfide, ether, amine and sulfone derivatives, Rapid Commun. Mass Spectrom. 11 (3) (1997) 316–320.
[19] P.-H. Lambert, S. Bertin, J.-M. Lacoste, J.-P. Volland, A. Krick, E. Furet, A. Botrel, P. Guenot, Electron ionization-induced loss of SO2 from 2-nitrodiaryl sulfides, J. Mass Spectrom. 33 (3) (1998) 242–249.
[20] M.L. Gross, Tandem mass spectrometry: multisector magnetic instruments, in: J.A. McCloskey (Ed.), Methods in Enzymology, 193, Academic Press, San Diego, 1990, pp. 131–153.
[21] J.J.P. Stewart, J.S. Frank, Optimization of parameters for semiempirical methods I, Method. J Comp. Chem. 10 (1989) 209–220.
[22] J.J.P. Stewart, J.S. Frank, Optimization of parameters for semiempirical methods. II. Applications, J. Comp. Chem. 10 (1989) 221–264.
[23] J.M. Wittbrodt, H.B. Schlegel, Some reasons not to use spin projected density functional theory, J. Chem. Phys. 105 (1996) 6574–6577.
[24] J. Baker, A. Scheiner, J. Andzelm, Spin contamination in density functional theory, J. Chem. Phys. Lett. 216 (1993) 380–388.
[25] G.J. Laming, N.C. Hardy, R.D. Amos, Kohn–Sham calculation on open-shell diatomic molecules, Mol. Phys. 80 (1993) 1121–1134.
[26] A. Nicolaides, D.M. Smith, F. Jensen, L.J. Radom, Phenyl radical, cation, and anion, the triplet-singlet gap and higher excited states of the phenyl cation, J. Am. Chem. Soc. 119 (1997) 8083–8088.
[27] M.J. Frisch, G.W. Trucks, H.B. Schlegel, G.E. Scuseria, M.A. Robb, J.R. Cheeseman, J.A. Montgomery Jr., T. Vreven, K.N. Kudin, J.C. Burant, J.M. Millam, S.S. Iyengar, J. Tomasi, V. Barone, B. Mennucci, M. Cossi, G. Scalmani, N. Rega, G.A. Petersson, H. Nakatsuji, M. Hada, M. Ehara, K. Toyota, R. Fukuda, J. Hasegawa, M. Ishida, T. Nakajima, Y. Honda, O. Kitao, H. Nakai, M. Klene, X. Li, J.E. Knox, H.P. Hratchian, J.B. Cross, C. Adamo, J. Jaramillo, R. Gomperts, R.E. Stratmann, O. Yazyev, A.J. Austin, R. Cammi, C. Pomelli, J.W. Ochterski, P.Y. Ayala, K. Morokuma, G.A. Voth, P. Salvador, J.J. Dannenberg, V.G. Zakrzewski, S. Dapprich, A.D. Daniels, M.C. Strain, O. Farkas, D.K. Malick, A.D. Rabuck, K. Raghavachari, J.B. Foresman, J.V. Ortiz, Q. Cui, A.G. Baboul, S. Clifford, J. Cioslowski, B.B. Stefanov, G. Liu, A. Liashenko, P. Piskorz, I. Komaromi, R.L. Martin, D.J. Fox, T. Keith, M.A. Al-Laham, C.Y. Peng, A. Nanayakkara, M. Challacombe, P.M.W. Gill, B. Johnson, W. Chen, M.W. Wong, C. Gonzalez, J.A. Pople, Gaussian 03, Revision C. 02, Gaussian Inc., Wallingford CT, 2004.
[28] M.J. Frisch, G.W. Trucks, H.B. Schlegel, G.E. Scuseria, M.A. Robb, J.R. Cheeseman, V.G. Zakrzewski, J.A. Montgomery Jr., R.E. Stratmann, J.C. Burant, S. Dapprich, J.M. Millam, A.D. Daniels, K.N. Kudin, M.C. Strain, O. Farkas, J. Tomasi, V. Barone, M. Cossi, R. Cammi, B. Mennucci, C. Pomelli, C. Adamo, S. Clifford, J. Ochterski, G.A. Petersson, P.Y. Ayala, Q. Cui, K. Morokuma, D.K. Malick, A.D. Rabuck, K. Raghavachari, J.B. Foresman, J. Cioslowski, J.V. Ortiz, B.B. Stefanov, G. Liu, A. Liashenko, P. Piskorz, I. Komaromi, R. Gomperts, R.L. Martin, D.J. Fox, T. Keith, M.A. Al- Laham, C.Y. Peng, A. Nanayakkara, C. Gonzalez, M. Challacombe, P.M.W. Gill, B. Johnson, W. Chen, M.W. Wong, J.L. Andres, C. Gonzalez, M. Head-Gordon, E.S. Replogle, J.A. Pople, Gaussian 98, Revision A. 6, Gaussian Inc., Pittsburgh, PA, 1998.
[29] A.P. Scott, L. Radom, Harmonic vibrational frequencies: an evaluation of Hartree-Fock, Møller–Plesset, quadratic configuration interaction, density functional theory, and semiempirical scale factors, J. Phys. Chem. 100 (1996) 16502–16513.
[30] Leonard, J. Nelson, Johnson, R. Carl, Periodate oxidation of sulfides to sulfoxides. Scope of the reaction, J. Org. Chem. 27 (1962) 282–284.